# *AstroSat/UVIT* observations of IC 4329A: constraining the accretion disc inner radius

Gulab C. Dewangan [1]★ P. Tripathi [1] I. E. Papadakis[2,3] and K. P. Singh[4]

[1]*Inter-University Centre for Astronomy and Astrophysics (IUCAA), SPPU Campus, 411007, Pune, India*
[2]*Department of Physics and Institute of Theoretical and Computational Physics, University of Crete, 71003 Heraklion, Greece*
[3]*Institute of Astrophysics - FORTH, N. Plastira 100, 70013 Vassilika Vouton, Greece*
[4]*Department of Physcal Sciences, Indian Institute of Science Education and Research Mohali, Knowledge City, Sector 81, Manauli P.O., SAS Nagar, 140306 Punjab, India*

## ABSTRACT
We present a study of far- and near ultraviolet (UV) emission from the accretion disc in a powerful Seyfert 1 galaxy IC 4329A using observations performed with the *Ultraviolet Imaging Telescope* (*UVIT*) onboard *AstroSat*. These data provide the highest spatial resolution and deepest images of IC 4329A in the far- and near UV bands acquired to date. The excellent spatial resolution of the UVIT data has allowed us to accurately separate the extended emission from the host galaxy and the AGN emission in the far- and near UV bands. We derive the intrinsic AGN flux after correcting for the Galactic and internal reddening, as well as for the contribution of emission lines from the broad and narrow-line regions. The intrinsic UV continuum emission shows a marked deficit compared to that expected from the 'standard' models of the accretion disc around an estimated black hole mass of $1 - 2 \times 10^8 \, \mathrm{M_\odot}$ when the disc extends to the innermost stable circular orbit. We find that the intrinsic UV continuum is fully consistent with the standard disc models, but only if the disc emits from distances larger than $\sim$80–150 gravitational radii.

**Key words:** accretion, accretion discs – galaxies: active – galaxies: individual: IC 4329A – galaxies: Seyfert – ultraviolet: galaxies.

## 1 INTRODUCTION

The main ingredient of the accretion process responsible for the extraordinary luminosity of active galactic nuclei (AGN) is the presence of an accretion disc around a supermassive black hole (BH) at the centre of an active galaxy. Observationally, the accretion disc emission is believed to be responsible for the Big Blue Bump continuum spectral component (Malkan 1983; Czerny & Elvis 1987; Elvis et al. 1994; Koratkar & Blaes 1999; Shang et al. 2005). This component extends from near-infrared at $\sim$1 $\mu$ to far- and extreme-UV at $\sim$1000 Å, and accounts for more than half of the bolometric luminosity in type 1 AGN. However, the nature of the accretion discs in AGN is not as clear as in the case of BH X-ray binaries where the optically thick and geometrically thin standard accretion disc models have been successful (Davis, Done & Blaes 2006; McClintock & Remillard 2006). A great deal of complexity in AGN arises due to a number of effects such as contamination from host galaxy and numerous emission lines from the broad and narrow-line regions (NLRs), intrinsic extinction, lack of high quality UV data, etc.

Observations of relativistically broadened iron K$\alpha$ line and the related X-ray reflection emission from a number of AGN have indirectly revealed the presence of optically thick material in the form of discs around supermassive BHs (e.g. Fabian et al. 2000; Miller 2007). These observations, however, cannot probe the radial

dependence of the temperature and emission spectrum that are essential to unravel the nature of the accretion discs in AGN. Thus, the study of the intrinsic UV emission is crucial to probe the accretion discs in AGN. The *Ultraviolet Imaging Telescope* (*UVIT*; Tandon et al. 2017, 2020) on-board the *AstroSat* mission (Singh et al. 2014) with far- and near UV sensitivity and excellent spatial resolution (full width at half-maximum [FWHM] $\sim$1–1.5 arcsec), provides a unique opportunity to probe the intrinsic accretion disc emission from nearby AGN.

We studied the UV emission from the IC 4329A active nucleus using *AstroSat*/UVIT observations. IC 4329A is a nearby Seyfert 1.2 AGN (Véron-Cetty & Véron 2006) at a redshift of $z = 0.016\,054$ (Willmer et al. 1991). It is the second brightest type 1 AGN after NGC 4151 in the Swift/BAT catalogue (Baumgartner et al. 2013). The AGN resides in an edge-on galaxy with a dust lane passing through the nucleus. Based on a detailed multiwavelength spectral study, Mehdipour & Costantini (2018) estimated an accretion rate of $10 - 20$ per cent of the Eddington rate given its BH mass in the range of $1$–$2 \times 10^8 \, \mathrm{M_\odot}$. IC 4329A is extensively studied in the X-ray band by all major satellites e.g. *Einstein* (Petre et al. 1984; Holt et al. 1989), *EXOSAT* (Singh, Rao & Vahia 1991), *Ginga* (Piro, Yamauchi & Matsuoka 1990), *ASCA/RXTE* (Done, Madejski & Życki 2000), *BeppoSAX* (Perola et al. 2002), *Chandra* (McKernan & Yaqoob 2004), *XMM-Newton* (Nandra et al. 2007), *Suzaku* (Mantovani, Nandra & Ponti 2016), and most recently with *NuSTAR* (Brenneman et al. 2014).

We describe our *AstroSat* observations and data reduction in Section 2, followed by imaging analysis and derivation of intrinsic

★ E-mail: gulabd@iucaa.in

**Table 1.** AstroSat/*UVIT* observations of IC 4329A.

| Obs. ID | Date | Exposure time (ks) | |
|---|---|---|---|
| | | FUV/F154W | NUV/N245M |
| 9000001006 | 2017-02-03 | 18.8 | 17.2 |
| 9000001048 | 2017-02-23 | 18.1 | 20.0 |
| 9000001118 | 2017-03-29 | 19.5 | 19.6 |
| 9000001286 | 2017-06-11 | 18.2 | 18.8 |
| 9000001340 | 2017-06-25 | 12.4 | 18.4 |

AGN emission in Section 3. We derive the accretion disc spectra in Section 4 and discuss our results in Section 5.

## 2 OBSERVATIONS & DATA REDUCTION

IC 4329A was observed with *AstroSat* five times during February to June 2017 (Table 1). Here we present the data from the *UVIT*, which was operated in the Photon-Counting mode using two broadband filters: FUV/BaF2 (F154W, $\lambda_{mean}$ = 1541Å, $\Delta\lambda$ = 380Å) and NUV/NUVB13 (N245M, $\lambda_{mean}$ =2447Å, $\Delta\lambda$ = 280Å). We obtained the `level1` data from the *AstroSat* data archive,[1] and processed them using the *UVIT* pipeline CCDLAB (Postma & Leahy 2017). We generated cleaned images for each observation and merged the five images for each filter to increase the signal-to-noise ratio. The net exposure time of the resulting image is 94 ks (NUV) and 87 ks (far-UV [FUV]). We derived the astrometric solution transforming the image coordinates to the world coordinates using the ASTRONOMY.NET package (Lang et al. 2010).

We show the NUV and FUV images in Fig. 1 (upper panels). The edge-on host galaxy is seen in both images. A dust lane also appears, passing through the central nucleus. This is also observed with *HST* (Mehdipour & Costantini 2018). We did not detect the active nucleus in the FUV image. In order to find its position in this image, we generated a composite three-colour image using the FUV and NUV data, as well as X-ray data from *Chandra*. We obtained the publicly available *Chandra*/HETG data acquired from the observation performed on 2017 June 6 (observation ID:20070) and generated the zero order X-ray image from the `level2` event file. The composite colour image is shown in Fig. 1 (lower panel). The position of the bright nucleus in the X-ray and near UV band indicates that the dust lane in the host galaxy passes over the nucleus, and obscures its emission in the far-UV band. Based on the astrometry and the composite three colour image, we identify the location of the AGN in the FUV image that we use to generate the radial profile below.

## 3 DATA ANALYSIS

The observed UV/optical emission from active galaxies not only consists of the intrinsic accretion disc emission but it also includes emission from the host galaxy, the broad and NLR, the Fe II emission complex, and the Balmer continuum. In addition, the observed flux is also affected by the internal and the Galactic extinction. Below we describe the steps we followed to derive the intrinsic continuum emission.

### 3.1 Host galaxy contribution

In the UV band, dust extinction and star forming regions in spiral galaxies result in highly uneven and structured surface brightness in the observed images. It is difficult to model such structured 2D surface brightness profiles with smooth model profiles. On the other hand, averaging the galaxy emission over all azimuthal angle results in a reasonably smooth radial profile, which can be used to model the host galaxy and AGN profiles reliably. We separated the AGN emission from the host galaxy emission by fitting the radial surface brightness profile of IC 4329A with a galactic and a point source profile. We generated the radial profile of a star (see below) and the galaxy by considering the total number of counts per unit area in a large number of annular regions centred at each source position, up to a distance of 40 arcsec (this is necessary in order to determine well the background level in the galaxy radial profile). We used SHERPA (Freeman, Doe & Siemiginowska 2001) to fit the radial profiles, and we quote $1\sigma$ errors on the best-fitting parameters, corresponding to 68 per cent confidence level.

We first derived the radial profile of a point source. For the NUV band, we chose the star TYC 7279–861–1 ($\alpha_{2000}$ = 13h49m38.6, $\delta_{2000}$ = −30d18m04.1s), which is located outside the central region of the two images, shown in Fig. 1. This star is ∼4.2 arcmin away from IC 4329A, which is well isolated and bright enough for the radial profile analysis. TYC 7279–861–1 is faint in the FUV band, therefore we chose star CD−29 10609 ($\alpha_{J2000}$ = 13h48m57.8s, $\delta_{J2000}$ = −30d22m04.7s) in the FUV band, which is ∼5.75 arcmin away from IC 4329A. This star is bright enough in the FUV band for the radial profile analysis. We also derived radial profiles for other point-like sources, and we verified that they have similar radial profiles. We derived the point spread function (PSF) of the instrument by fitting the radial profile of the point sources with a circular Moffat function: $f(r) = A_M(1 + (\frac{r}{\gamma})^2)^{-\alpha}$, and a constant, $c_0$, for the background. We accept the FWHM of this function as a measure of the instrumental resolution (FWHM = $2\gamma\sqrt{2^{1/\alpha} - 1}$). We used the best-fitting parameters of the Moffat function (Table 2), and we calculated the FWHM of the PSF to be 1.2 arcsec for the NUV/NUVB13 and 1.5 arcsec for the FUV/BaF2 filters. These values are similar to that reported by Tandon et al. (2017, 2020). UVIT has superior spatial resolution compared to Swift/UVOT (∼2.5 arcsec FWHM; Breeveld et al. 2010) and *XMM-Newton*/OM (∼2 arcsec FWHM; Page et al. 2012) in the UV band.

We used the best-fitting Moffat function with variable nomalization to fit the nuclear emission from IC 4329A. We also used an exponential profile, $I(r) = A_E\exp(\xi r)$, and an off-centred Gaussian profile, $I(r) = A_G\exp(-\frac{4\log(2)(r-r_0)^2}{FWHM^2})$, to model the host galaxy radial profile. As before, we used a constant for the background.

The Gaussian profile is necessary to account for the off-centred peak emission that is clearly observed in the FUV image. This could be due to emission by an additional, off-centred star forming region but, most probably, the off-centred peak in the radial profile appears due to the obscuration by the central dust lane, and the rapid decline in the host galaxy emission away from the centre. If there was no obscuration, the galaxy profile would probably be well fitted by a single, exponential component. Now, with the obscuration due to the central dust lane, the off-centred Gaussian is necessary to account for the effects of the obscuration in the central part.[2] In the NUV

---

[1] https://astrobrowse.issdc.gov.in/astro_archive/archive/Home.jsp

[2] We note that our objective is not the study of the intrinsic properties of the host galaxy, therefore we do not fit the radial profile with an absorbed exponential profile but we separate the absorbed AGN emission from the host galaxy.
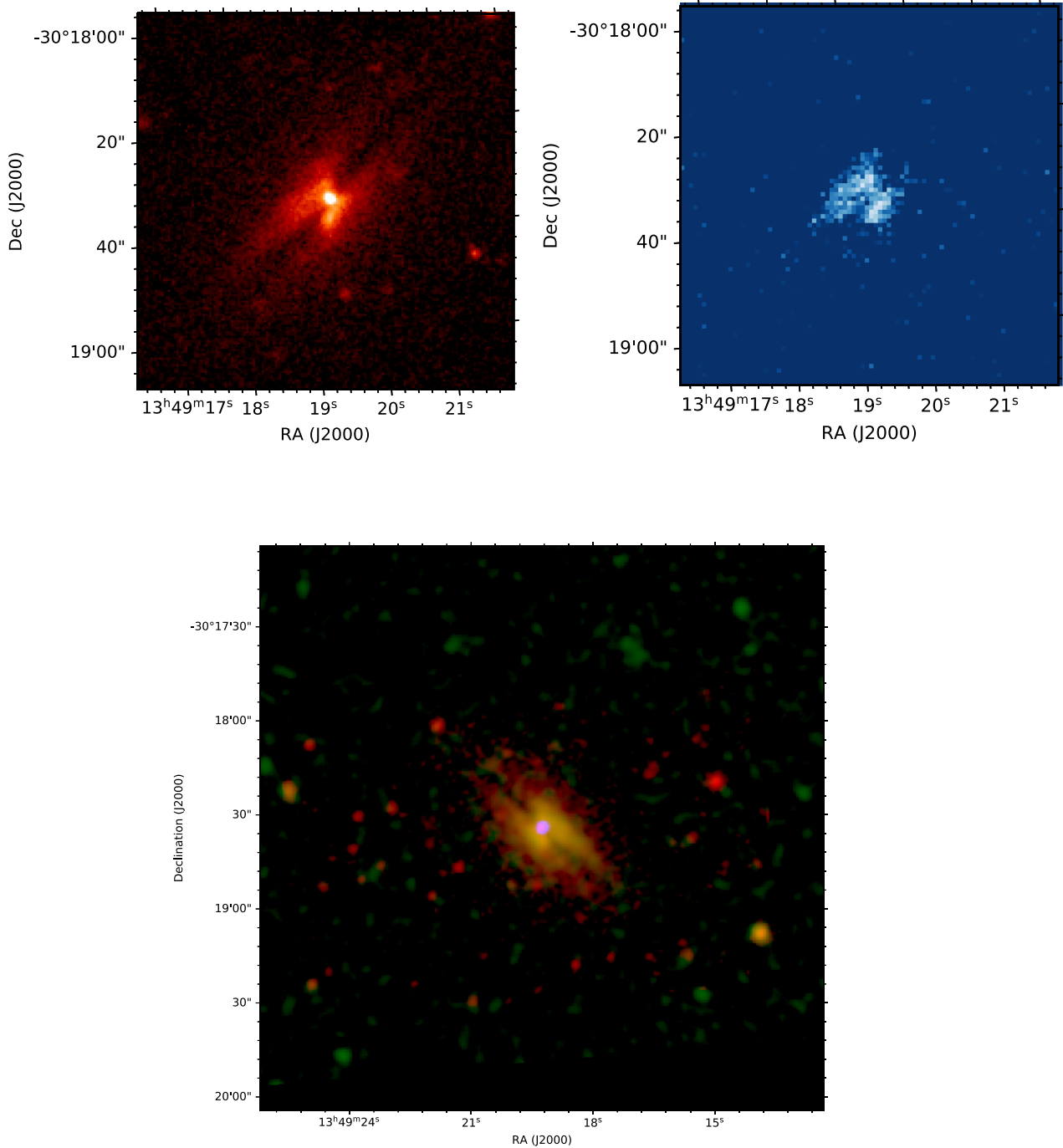
**Figure 1.** *Upper panels:* The NUV and FUV *AstroSat*/UVIT images of IC 4329A (left-hand and right-hand panel, respectively). The unresolved active nucleus is clearly seen in the NUV but not in the FUV band due to heavy extinction by the dust lane in the host galaxy passing through the central regions. *Bottom panel:* Composite *AstroSat*/UVIT NUV (red), FUV (green), and *Chandra* X-ray (blue) image of IC 4329A. The nucleus is clearly detected in X-rays as well.

band, the host galaxy is much brighter, due to significantly less obscuration and its stronger intrinsic flux. Therefore, an exponential gives a statistically good fit to the observed radial profile.

The set of model components listed in Table 2 resulted in a statistically good fit to the radial profile of IC 4329A in both the FUV and NUV bands. The parameters of the best-fitting models are listed in Table 2. The radial profiles and the best-fitting models are shown in Fig. 2. The best-fitting Moffat amplitude is $0 \pm 10.8$ counts arcsec$^{-2}$ in the FUV band. This result shows that the AGN is not detected in

this band (see also the upper right panel in Fig. 1). We list the $3\sigma$ upper limit on the Moffat amplitude in the last column of Table 2.

We calculated the AGN count rate in each band by integrating the best-fitting Moffat function within a 25 arcsec radius. We consider the $3\sigma$ upper limit on the Moffat normalization when calculating the FUV count rate. We converted the count rates to monochromatic flux densities using the unit conversion factors derived from the calibration (Tandon et al. 2017, 2020). The observed count rates and flux are listed in Table 3.

**Table 2.** Results from the radial profile analysis of IC 4329A.

| Model parameter | | NUV | | FUV | |
|---|---|---|---|---|---|
| | | Star | IC 4329A | Star | IC 4329A |
| Moffat | $\alpha$ | $1.81 \pm 0.05$ | $1.81(f)$ | $2.05 \pm 0.08$ | $2.05(f)$ |
| | $\gamma$ | $0.88 \pm 0.03$ | $0.88(f)$ | $1.18 \pm 0.05$ | $1.18(f)$ |
| | $A_m^a$ | $2792.7 \pm 79.7$ | $2461.3 \pm 41.1$ | $1621.0 \pm 48.7$ | $<32.5$ ($3\sigma$ upper-limit) |
| Constant | $c_0^a$ | $46.8 \pm 0.2$ | $46.8(f)$ | $18.3 \pm 0.1$ | $18.3(f)$ |
| Exponential | $\xi$ | – | $-0.208 \pm 0.005$ | – | $-0.19 \pm 0.01$ |
| | $A_e^a$ | – | $462.8 \pm 13.8$ | – | $61.0 \pm 8.5$ |
| Gaussian | $x_0$ | – | – | – | $3.0 \pm 0.2$ |
| | FWHM | – | – | – | $4.2 \pm 0.5$ |
| | $A_G^a$ | – | – | – | $39.0 \pm 3.3$ |
| | $\chi^2/dof$ | $104.6/96$ | $169.1/195$ | $59.0/86$ | $181.5/174$ |

$^a$In units of counts arcsec$^{-2}$.
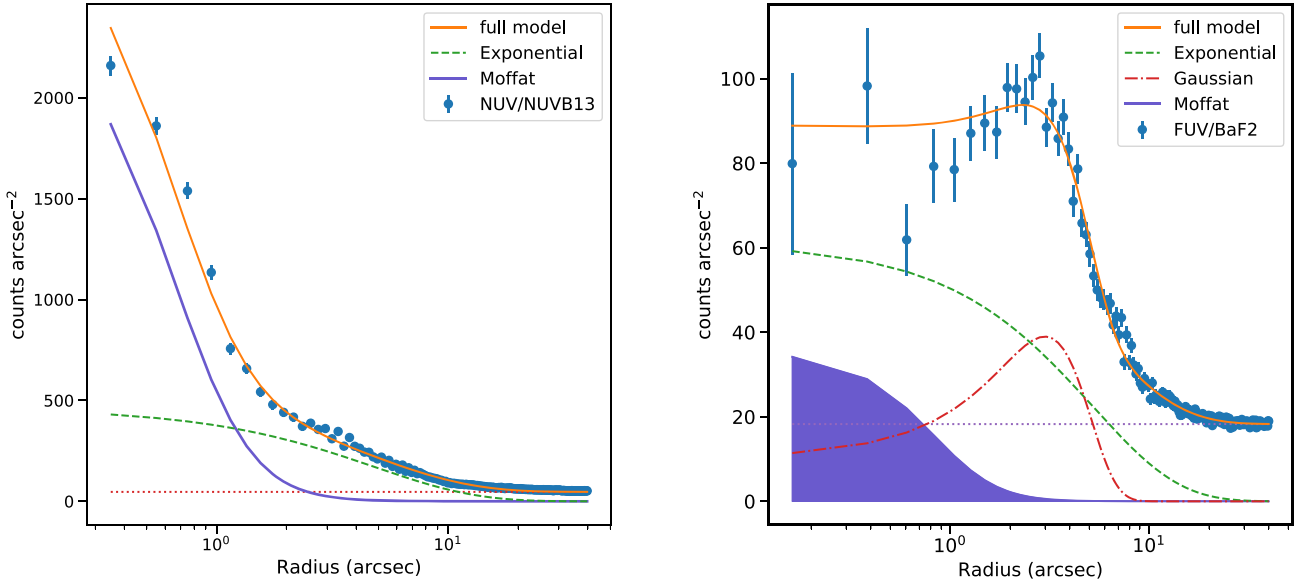


**Figure 2.** Radial profile of IC 4329A derived from the merged *AstroSat*/NUV (*left*) and FUV (*right*) images. The radial profiles are fitted with the instrument PSF for the AGN, and an exponential function for the galaxy emission plus a Gaussian function to account for the extra emission detected in the FUV band, probably due to the central star-forming region. The AGN is not detected in the FUV band, and the shaded region in the right-hand panel shows the $3\sigma$ upper limit on the AGN contribution. The deficit in the FUV emission in the central region is due to the the dust lane passing through the centre of the galaxy.

**Table 3.** Far and near UV flux measurements of IC 4329A.

| Quantity | Extinction law | $E(B-V)$ | NUV | FUV |
|---|---|---|---|---|
| | – | – | | ($3\sigma$ upper limit) |
| Net AGN counts s$^{-1}$ | – | – | $0.078 \pm 0.001$ | $<0.0015$ |
| Observed $f_\lambda^a$ | – | – | $(5.7 \pm 0.1) \times 10^{-2}$ | $<5.6 \times 10^{-3}$ |
| Intrinsic$^b$ cont. $f_\lambda^a$ | Czerny et al. (2004) | (0.8, 1.0) | $(7.0 \pm 1.1, 31.4 \pm 0.5)$ | ($<6.3, <35.2$) |
| | Gaskell & Benker (2007) | 0.97 | $28.2 \pm 0.5$ | $<11.3$ |
| | Calzetti et al. (2000) | 1.07 | $173.5 \pm 3$ | $<163.5$ |

$^a$In units of $10^{-15}$ ergs cm$^{-2}$ s$^{-1}$ Å$^{-1}$.
$^b$Flux derived after de-reddening due to the Galactic and internal extinction, and after correcting for the contribution of emission lines.

## 3.2 Corrections for the galactic and internal extinction

A significant amount of flux in the UV/optical bands may be absorbed and scattered by the interstellar dust grains both in the host galaxy as well as in the interstellar medium of the Milky Way. We corrected for the Galactic extinction using the extinction curve of Cardelli, Clayton & Mathis (1989). We used the line-of-sight colour excess $E(B-V) = 0.052$ from Schlafly & Finkbeiner (2011) and fixed the ratio of total to selective extinction $R_V = \frac{A_V}{E(B-V)} = 3.1$. As is obvious from the central dust lane, the emission from the AGN in IC 4329A suffers significant internal extinction. We describe below how we computed the unobscured intrinsic flux of the active nucleus.

First, we corrected for the internal reddening using the extinction curve of Czerny et al. (2004) that lacks the 2175 Å bump and is flatter than that of the Milky Way. This extinction curve was constructed based on the blue and red composite quasar spectra, and is found to be appropriate for reddened AGN (Mehdipour, Branduardi-Raymont & Page 2012; Mehdipour & Costantini 2018) including IC 4329A.

The internal reddening can be determined based on the Balmer decrement i.e. the ratio of the observed flux of the Balmer lines H$\alpha$ to H$\beta$. Three measurements (Marziani, Calvani & Sulentic 1992; Winge et al. 1996; Malkan et al. 2017) in the last 30 yr show that the Balmer decrement in IC 4329A is in the range of 8.85–9.5. For $R_V = 3.1$, the Czerny et al. extinction law leads to the relation between reddening and the Balmer decrement, $E(B - V) = 1.475 \log(R_{obs}/R_{int})$, where $R_{obs}$ and $R_{int}$ are the observed and intrinsic H$\alpha$/H$\beta$ ratios. We used $R_{int} = 2.72$, which is a value derived for observations of unreddened AGN (Gaskell 2017). For $R_{obs} = 8.85$–9.5, we found $E(B - V) = 0.75$–0.8 for IC 4329A. We adopt the internal reddening of $E(B - V) = 0.8$ based on the largest value of Balmer decrement. By fitting the broadband continuum from IR to near UV, Mehdipour & Costantini (2018) measured an internal extinction of $E(B - V) = 1.0 \pm 0.1$ for IC 4329A. Hence, we also used $E(B - V) = 1.0$ and derived two sets of intrinsic flux for $E(B - V) = 0.8$ and 1.0.

We also considered the extinction curve of Gaskell & Benker (2007) found to be appropriate for AGN (Czerny 2007). For this curve, the relation between the reddening and the Balmer decrement can be written as $E(B - V) = 1.79 \log(R_{obs}/R_{int})$ for $R_V = 3.1$. Using $R_{obs} = 9.5$ and $R_{int} = 2.72$, we derived $E(B - V) = 0.97$ that we used to de-redden the observed flux. The presence of dust lane and UV emission from the host galaxy suggests strong star formation. Thus, the attenuation of AGN light in IC 4329A may be due to dusty environment in the central star-forming region, within the host galaxy. Therefore, we also used the extinction of law of Calzetti et al. (2000) derived for local starburst galaxies. We found $E(B - V) = 1.07$ for $R_{obs} = 9.5$ and $R_{int} = 2.72$, using the relation $E(B - V) = 1.94 \log(R_{obs}/R_{int})$ for $R_V = 4.05$ derived from the Calzetti et al. (2000) extinction law.

### 3.3 Correction for emission-line contribution

Emission lines from the narrow-line and the broad-line region, including the mFe II emission and Balmer continuum, may contribute significantly to the flux measured with broadband filters in the optical/UV range. In our case, the broad emission lines due to Si IV, C IV, and Fe II contribute predominantly to emission in the FUV/F154W filter bandpass, while the Balmer continuum and Fe II emission contribute to the NUV/N245M bandpass.

To subtract the contributions from these components, we used the composite quasar spectrum (CQS) derived by Vanden Berk et al. (2001). We fitted a power-law model to the line-free 1350–1365 and 4200–4230 Å bands in the CQS, and derived the intrinsic continuum. The CQS shifted to the redshift of IC 4329A and the best-fitting double power-law continuum are shown in Fig. 3. Also, shown are the effective areas of the broadband filters FUV/F154W and NUV/N245M.

We subtracted the best-fitting continuum and derived the pure emission-line spectrum. We then calculated the expected count rates in the FUV/F154W and NUV/N245M filters for both the emission-line spectrum and the CQS using the effective areas for the two filters. We thus calculated that emission lines contribute 17.7 per cent and 17.4 per cent to the total intrinsic flux in the FUV/F154W and
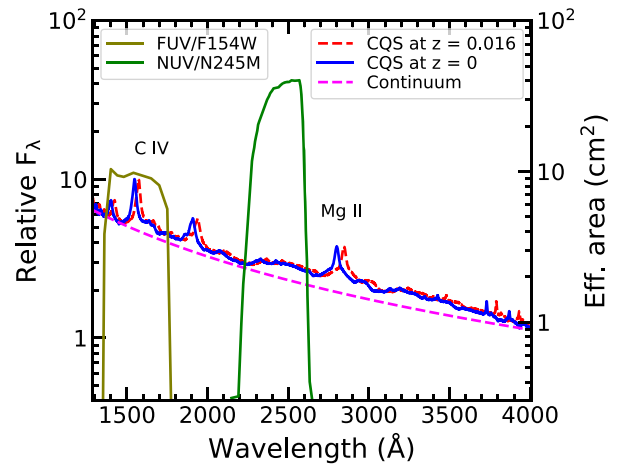


**Figure 3.** The CQS of Vanden Berk et al. (2001) shifted to match the redshift of IC 4329A. Also shown are the effective areas of FUV/F154W and NUV/N245M (Tandon et al. 2020). The dashed line shows the continuum that was used to derive the contribution of emission lines in the two broadband filters.

NUV/N245M bands, respectively. We used these contributions to correct for the contribution of the emission lines to the intrinsic UV flux of IC 4329A. Thus derived the intrinsic continuum flux density in the two filters (de-reddened, for all three extinction laws we considered, and free of host galaxy and emission lines contribution), are listed in Table 3.

### 4 THE UV/OPTICAL SPECTRUM OF IC 4329A

We plot the intrinsic AGN flux in the far- and near UV bands as a function of wavelength in all panels of Fig. 4. The results for the Czerny et al. (2004), Gaskell & Benker (2007), and the Calzetti et al. (2000) extinction curves are plotted in the upper, lower left, and lower right panels, respectively. Filled and open points in the upper panels show the flux measurements for the Czerny et al. (2004) extinction curve derived for $E(B - V) = 0.8$ and 1.0, respectively. Squares in all panels of Fig. 4 show the mean intrinsic flux at 5100 Å based on measurements by Bentz et al. (2009). These authors used a high-resolution *HST* image to decompose the galaxy contribution from the AGN emission. They corrected the data for Galactic reddening, and applied all the additional corrections as we did to the *UVIT* data. They list the mean AGN flux using data from ground based, spectroscopic monitoring campaigns, thus taking into account the intrinsic variability of the source. In any case, the optical variability amplitude of IC 4329A is of the order of few per cent around the mean (Mehdipour & Costantini 2018). Therefore, we can safely combine our and the Bentz et al. (2009) measurements together, to construct the optical/UV spectral energy distribution (SED) of the source.

The BH mass of IC 4329A has been estimated to be in the range of ∼1–2 × 10$^8$ M$_\odot$ (Markowitz 2009; de La Calle Pérez et al. 2010; Vasudevan et al. 2010). We assumed $M_{BH} = 1.5 \times 10^8$ M$_\odot$ and we computed spectra of standard discs for accretion rates in the range between $\log \dot{m} = -3$ and $-1$, with a step of $\Delta \dot{m} = 0.1$ (accretion rates are normalized to the Eddington accretion rate). We used the model OPTXAGNF (Done et al. 2012) available in the XSPEC program (version 12.11.1; Arnaud 1996 distributed with the HEASOFT package
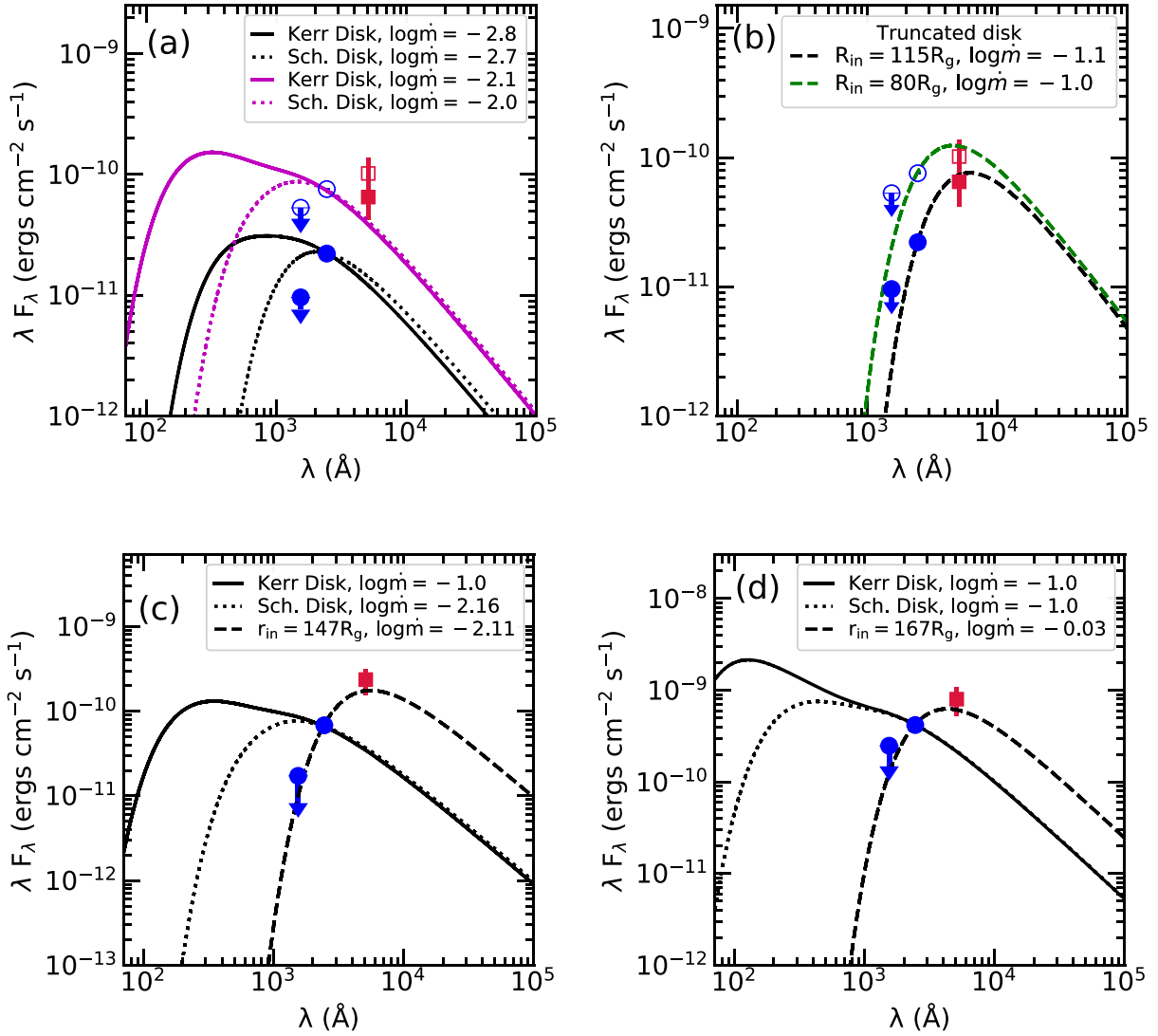
**Figure 4.** The intrinsic, far-, and near UV flux measured with *AstroSat/UVIT* (circles) and the optical flux at 5100 Å based on the measurement of by Bentz et al. (2009; squares). The intrinsic AGN flux was derived using the extinction curves of Czerny et al. (2004; a and b), Gaskell & Benker (2007; c), and Calzetti et al. (2000; d). In the case of the Czerny et al. extinction law, the intrinsic UV/optical fluxes were derived for $E(B - V) = 0.8$ (filled symbols) and $E(B - V) = 1.0$ (open symbols). Solid and dotted lines show theoretical accretion disc spectra when $R_{in} = R_{ISCO}$, in the case of a maximally rotating and a non-rotating, Schwarzschild BH, respectively. The dashed lines show the theoretical spectra when the inner disc radius is larger than $R_{ISCO}$. Accretion rates (in Eddington limit units) and the inner disc radius listed in the inset box are those that give the best fit to the data (see text for details).

(version 6.28), to calculate the disc spectra.[3] The model assumes that the gravitational energy released in the disc at each radius is emitted as a (colour temperature corrected) blackbody using the Novikov–Thorne prescription (Novikov & Thorne 1973).

First, we considered the case when the inner disc radius, $R_{in}$, is equal to $R_{ISCO}$, i.e. the radius of the innermost stable circular orbit (ISCO) for a maximally spinning Kerr BH and a non-rotating Schwarzschild BH ($R_{ISCO} = 1.235\,R_g$ and $R_{ISCO} = 6\,R_g$, respectively; $R_g = GM_{BH}/c^2$ is the gravitational radius). The solid and dashed lines in Fig. 4 show the disc spectra in the two cases. The model disc spectra shown are the ones with the minimum difference (squared) with the data (including the upper limit in the far-UV). The standard disc

extending to ISCO fails to explain the observed data. As expected, due to the $\nu^{1/3}$ dependency, the theoretical accretion disc spectra rise towards shorter wavelength while the observed data show the opposite trend. They show a steady flux decline, from the optical to the far-UV, which is strongly emphasized by the upper limit in the FUV band.

The discrepancy between the standard disc model and the data holds for all the different extinction laws we tried. Perhaps we can get a better agreement between the model and the observations if we assume a larger $E(B - V)$. Absorption by dust should affect the FUV band more than the NUV/optical bands. If we increase $E(B - V)$, the FUV upper limit will increase more than the NUV/optical flux measurements, and perhaps the data will be consistent with theory. We estimate $E(B - V)$ assuming $R_{int} = 2.72$, which is a value consistent with theoretical calculations where the gas is optically thick in Lyman lines, in which case $H\alpha/H\beta \approx 2.85$ (Baker & Menzel
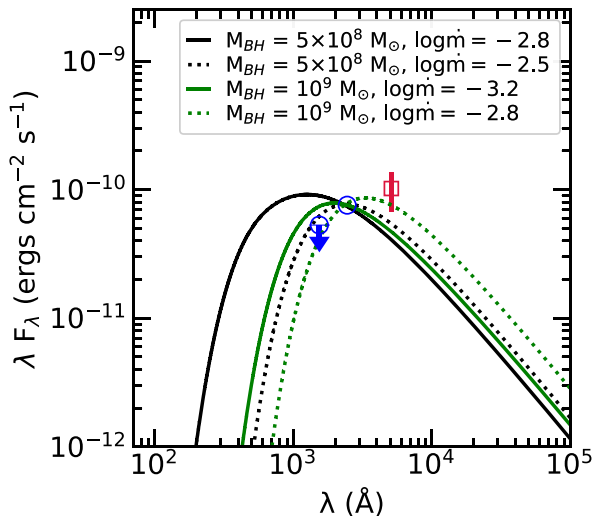
---

[3]We set the model parameter $r_{cor}$ equal to minus the inner disc radius to calculate only the disc spectrum.

**Figure 5.** The Kerr (solid curves) and the Schwarzschild (dotted curves) accretion discs spectra for BH masses of $5 \times 10^8 \, M_\odot$ (black) and $10^9 \, M_\odot$ (green). AGN fluxes are corrected for the internal extinction using the extinction curve of Czerny et al. (2004) with a colour excess of $E(B - V) = 1.0$.

1938; Osterbrock & Ferland 2006). The intrinsic Balmer decrement can be different from one AGN to another, because it depends on the physical environment of the emission regions, e.g. hydrogen density. For example Fig. 4 in Gaskell (2017) shows that $R_{int} \approx 1.9$ when $\log N_H \geq 12$. But, even in this case, we get $E(B - V) \sim 1$ if assuming the Czerny et al. (2004) extinction curve for example, a case we have already considered in our calculations (empty points in the upper panels in Fig. 4).

OPTXAGNF is only an approximation of the disc emission in AGN. For one thing it does not include the relativistic effects in the inner disc region. These should be more pronounced in the case of maximally rotating BHs, where photons emitted from this region will suffer gravitational redshit, their trajectories will be strongly curved and may not reach the observer at infinity, etc. However, the discrepancy between model and data appear in a spectral region that should be relatively free of relativistic effects. The model spectra in the case of the maximally rotating and Schwarzschild BHs are identical below 1000 Å, for the BH mass we have assumed (see the solid and dotted lines in all panels of Fig. 4). This implies that the emission at these wavelengths is dominated by radii larger than $6 \, R_g$. In addition, the OPTXAGNF model does not include the inclination effects, but these should mainly cause a change in the model normalization (due to the change of the projected disc area at high inclinations), at least at wavelengths longer than 1000 Å, where the relativistic effects should be less pronounced. However, we find a disagreement between the model and the observed slope, not between the predicted and the observed normalization.

Another possibility is that the BH mass is quite larger than the one we considered. We therefore derived Kerr and Schwarzschild disc spectra for masses equal to $5 \times 10^8$ and $10^9 \, M_\odot$, and for various mass accretion rates. The spectra that describe best the data are shown in Fig. 5. Solid and dotted curves show the spectra for a maximally spinning and a non-rotating BH, respectively, while black and green colours show the spectra for the $M_{BH} = 5 \times 10^8 \, M_\odot$ and $M_{BH} = 10^9 \, M_\odot$. The figure shows that spectrum in the case of a Schwarzschild BH with a mass of $10^9 \, M_\odot$ describes the data well (green dotted spectrum), with an accretion rate of $\log \dot{m} = -2.8$.

However, this BH mass is almost ten times larger than all the other BH mass estimates for this galaxy (see for example the discussion on the BH mass estimation for this object in Mehdipour & Costantini (2018).

Finally, the discrepancy between standard disc models and the data suggests that the possibility of a truncated accretion disc is IC 4329A. We therefore generated theoretical spectra for accretion discs truncated at radii larger than $R_{ISCO}$. We computed disc models with with $R_{in}$ in the range between 50 and 200 $R_g$, in steps of $\Delta R_{in} = 1$, for the full range of the accretion rates we considered. The dashed lines in the right-hand panel of Fig. 4 show the best-fitting disc spectra in this case, for a Schwarzschild BH. These are the model curves which resulted in the smallest (squared) difference between model and data in the NUV and optical bands, and are also consistent with the upper limit in the FUV band. Clearly, the data are consistent with the spectrum emitted by truncated discs. The inner radius depends on the assumed intrinsic extinction curve, and ranges from $R_{in} \sim 80$ in the case of the Czerny et al. curve, to $R_{in} \sim 150$–$170 \, R_g$ when we assume the other two curves.

## 4.1 The inner disc

Our results clearly demonstrate that the standard accretion disc models are consistent with the data but only if $R_{in} \gtrsim 80$–$100 \, R_g$. The inner disc could be replaced by a hot, optically thin flow (see Mahmoud & Done 2020) or there could exist a warm, optically thick medium on top of the inner disc, as hypothesized in the thermal Comptonization models for the origin of the soft X-ray excess (see e.g. Done et al. 2012). In a companion paper, Tripathi et al. (2021) have studied the broadband (0.3–20 keV) X-ray spectra of IC 4329A acquired simultaneously with the *AstroSat* UV data presented here. They detected a soft-excess component, which can be fitted well either by a simple black-body component with $kT \sim 0.26$ keV, or by the thermal Comptonization model NTHCOMP, with a warm corona temperature of $kT_e \sim 0.26$ keV and an optical depth of $\tau \sim 27$. Their analysis also revealed that the fraction of the continuum X-ray power-law flux and the total X-ray flux (i.e. power-law plus soft-excess emission) to be $f_{PL} \sim 0.8$.

We used the parameters for the soft excess and the power-law fraction and we refitted the UV/optical data derived for the three different extinction curves with OPTXAGNF. We kept the OPTXAGNF parameters $kT_e$ and $\tau$, for the soft excess, and $f_{PL}$ fixed to the values derived by Tripathi et al. (2021). We found that the three optical/UV SEDs are well described by the model when the BH spin is fixed at $a = 0$, while we could not fit the data in the case of $a = 1$. The best-fitting results are $R_{in} \sim 126$ and $\sim 80$ for the extinction curve of Czerny et al. (2004) with $E(B - V) = 1.0$ and 0.8, and $R_{in} \sim 200$, 74 for the extinction curves of Calzetti et al. (2000) and Gaskell & Benker (2007), respectively.

Tripathi et al. (2021) also measured the soft excess flux in the 0.3–2 keV band. They found it to be variable, between 1.1 and $1.7 \times 10^{-10}$ ergs s$^{-1}$ cm$^{-2}$. We used the OPTXAGNF best-fitting models and we computed the model predicted soft-excess flux in the same energy range. We found that the best-fitting soft-excess flux predictions are off by at least a factor of two from the values measured by Tripathi et al. (2021), except for the extinction curve of Czerny et al. (2004) with $E(B - V) = 1.0$. In this case, the estimated soft excess flux in the 0.3–2 keV is within the range of the fluxes measured by Tripathi et al. (2021) from the five *AstroSat* observations. The best-fitting inner radius and accretion rate are $126 \, R_g$ and $\sim 2.4$ per cent of the Eddington rate, respectively. This suggests that the inner disc in IC 4329A could be covered by a

warm, optically thick layer, whose emission is consistent with the optical/UV SED and could also explain the observed soft-excess we detect in this source.

## 5 DISCUSSION AND CONCLUSIONS

We present the results from the analysis of UV images of IC 4329A obtained with *AstroSat*/*UVIT* observations. These are the highest resolution and deepest images of IC 4329A ever acquired with any telescope in the near and far-UV bands. The *UVIT* images enabled us to calculate the galaxy radial profile, and unambiguously separate the AGN emission from the extended emission of the host galaxy by fitting the profiles with the appropriate functions. We derived the intrinsic AGN continuum flux after de-reddening for both the Galactic and internal extinctions, and correcting for the contribution of emission lines.

The active nucleus is not detected in the FUV band, and we were able to put a conservative $3\sigma$ upper limit on the AGN flux in this band. When combined with the AGN flux in the NUV and 5100 Å (taken from past observations), we found that the far-UV/optical, intrinsic emission of the active nucleus in IC 4329A, requires no disc emission below $\sim 80$–$170\,R_g$. The superb spatial resolution of *UVIT* is crucial in this case, specially in the FUV. If we had performed simple aperture photometry in the FUV image, using a 5–10 arcsec radius (as is typically the case), we would have ended with a flux measurement at least seven times larger than the $3\sigma$ upper limit we have determined in this band. Since the host galaxy in most templates is assumed to emit very little at these short wavelengths, this measurement would have been assumed to be intrinsic of the active nucleus, and this false result would have critically altered the shape of the intrinsic AGN SED at short wavelengths.

X-ray reflection spectroscopy can independently probe the inner accretion discs via the relativistic iron K$\alpha$ line near $\sim 6.4$ keV and the strength of the reflection. Using *XMM-Newton* observations of IC 4329A, Nandra et al. (2007) derived a low-disc reflection fraction of $R_f \sim 0.3$ ($R_f$ is defined as the ratio of the X–ray intensity that illuminates the disc to the intensity that reaches the observer; $R_f = 1$ corresponds to a semi-infinite slab subtending $2\pi$ solid angle at the X-ray source). Using *NuSTAR* observations, Brenneman et al. (2014) detected a moderately broad iron line with a Gaussian $\sigma \sim 0.36$ keV in addition to narrow iron K$\alpha$, K$\beta$ lines. Ogawa et al. (2019) analysed simultaneous *Suzaku* and *NuSTAR* observations and showed that the iron line complex is well described by relativistic reflection from an accretion disc truncated at $R_{in} = 87^{+73}_{-13}\,R_g$ and distant reflection from a clumpy torus, with the relativistic reflection fraction $\sim 3 \times 10^{-3}$. In general, the reflection fraction is unlikely to go below $\sim 0.5$ for an accretion disc extending to the last stable orbit (Dauser et al. 2016). Hence, the moderately broad iron line and the low reflection fraction both support the hypothesis of a truncated disc in IC 4329A.

The deficit of the intrinsic UV emission can arise if the disc is truly truncated i.e. there is no optically thick material accreting in the inner regions to emit in the UV/optical bands. This is probably the case with Galactic, BH X-ray binaries, when they are in their quiescent and hard-state (see Esin, McClintock & Narayan (1997), Done, Gierliński & Kubota (2007), Mahmoud & Done (2020)). In this case, the inner disc is replaced by a hot, optically thin, Advection-Dominated Accretion Flow (ADAF)-like flow (Narayan & Yi 1994), which emits in X-rays. This could also be the case with low-luminosity AGN, like Low Ionisation Nuclear Emission Line Region galaxies (LINERS). However, this is supposed to happen when the accretion rate is below $\sim 1$–2 per cent of the Eddington limit. Our

truncated disc fits to the data indicate a higher accretion rate, of the order of 0.1, or more, depending on the assumed extinction curve.

Another possibility is that the inner disc in IC 4329A is covered by a warm layer ($kT \sim 0.2$–0.5 keV), with high optical depth of $\sim 10$–20. The idea of the warm, and optically thick corona, on top of the inner accretion disc, has been applied successfully to model the broad-band optical/UV/X-ray SEDs of several AGN (Magdziarz et al. 1998; Czerny et al. 2003; Jin et al. 2012; Mehdipour et al. 2015; Kubota & Done 2018; Porquet et al. 2018; Petrucci et al. 2020), although it is not certain yet whether such a layer/corona can exist in the upper layers of the inner accretion flow. If it does, and it is optically thick, all UV/optical photons emitted by the disc will be shifted to soft X-rays, resulting in a deficit in the observed UV/optical emission. We investigated this possibility by assuming the OPTXAGNF model and using the soft excess parameters derived by Tripathi et al. (2021). We found that the model predicted soft excess flux is consistent with the Tripathi et al. (2021) measurements only for one of the three extinction curves we considered. This is the Czerny et al. (2004) extinction curve, with $E(B - V) = 1$. This is in agreement with the results of Mehdipour & Costantini (2018). However, we infer an accretion ratio ratio of $\sim 2.4$ per cent of the Eddington limit, while Mehdipour & Costantini (2018) derived an accretion rate of $\sim 10 - 20$ per cent, in Eddington units. Perhaps the higher Eddington fraction could be the reason why the optical-FUV spectral shape derived by Mehdipour & Costantini (2018) is relatively flat compared to our measurements.

The main result of our work is that the optical to far-UV SED of IC 4329A is consistent with standard accretion disc models only if the inner disc does not contribute to the observed UV emission. The standard inner disc in IC 4329A is either replaced by some optically thin, hot inner flow, or it is covered by an optically thick, 'warm' X-ray corona. We cannot constrain $R_{in}$ and the accretion rate accurately, mainly because we do not know the exact extinction curve.

If we assume that the observed soft excess (Tripathi et al. 2021) is due to warm Comptonization, then we find that the extinction law is well described by Czerny et al. (2004) with $E(B - V) = 1$, the inner disc radius is $R \sim 125$, and the accretion rate is quite small ($\dot{m} \sim 0.025$). Recently Noda & Done (2018) have discovered that changing look AGN make spectral transitions at a few per cent of the Eddington luminosity between a faint state characterized by a truncated disc and a hot corona and a bright state requiring a warm corona in addition to a disc and a hot corona. In the case of IC 4329A, the disc truncation, the weakness of the soft excess component that contributes only $\sim 20$ per cent to the broadband X-ray emission, and the low Eddington fraction $\sim 2.5$ per cent for the Czerny et al. extinction law strongly suggest that this AGN is very near the spectral transition point described by Noda & Done (2018) for the changing-look AGN.

*AstroSat*/UVIT observations of AGN with negligible or known internal reddening will provide better constraints on the inner extent of the accretion discs. We plan to study the far- and near UV *AstroSat* data on a number of bright AGN, which will allow us to disentangle the *intrinsic* AGN emission from the host galaxy flux in the near and far-UV bands, and investigate the inner accretion flow in these objects.

archived at the Indian Space Science Data Centre (ISSDC). This publication uses *UVIT* data processed by the payload operations centre at IIA. The UVIT is built in collaboration between IIA, IUCAA, TIFR, ISRO, and CSA. This research has made use of the SIMBAD database, operated at CDS, Strasbourg, France. This research has made use of software provided by the Chandra X-ray Center (CXC) in the application package Sherpa. PT acknowledges the University Grant Commission (UGC), Government of India for financial supports.

## DATA AVAILABILITY

The Level-1 UVIT data from the five observations with IDs 9000001006, 9000001048, 9000001118, 9000001286, and 9000001340 used in this paper are publicly available at the *AstroSat* data archive https://astrobrowse.issdc.gov.in/astro_archive/archive/Home.jsp maintained by the ISSDC.

## REFERENCES

Arnaud K. A., 1996, in Jacoby G. H., Barnes J., eds, ASP Conf. Ser., Vol. 101, Astronomical Data Analysis Software and Systems V. Astron. Soc. Pac., San Francisco, p. 17
Baker J. G., Menzel D. H., 1938, ApJ, 88, 52
Baumgartner W. H., Tueller J., Markwardt C. B., Skinner G. K., Barthelmy S., Mushotzky R. F., Evans P. A., Gehrels N., 2013, ApJS, 207, 19
Bentz M. C., Peterson B. M., Netzer H., Pogge R. W., Vestergaard M., 2009, ApJ, 697, 160
Breeveld A. A. et al., 2010, MNRAS, 406, 1687
Brenneman L. W. et al., 2014, ApJ, 788, 61
Calzetti D., Armus L., Bohlin R. C., Kinney A. L., Koornneef J., Storchi-Bergmann T., 2000, ApJ, 533, 682
Cardelli J. A., Clayton G. C., Mathis J. S., 1989, ApJ, 345, 245
Czerny B., 2007, ASP Conf., 373, 586
Czerny B., Elvis M., 1987, ApJ, 321, 305
Czerny B., Nikołajuk M., Różańska A., Dumont A. -M., Loska Z., Zycki P. T., 2003, A&A, 412, 317
Czerny B., Li J., Loska Z., Szczerba R., 2004, MNRAS, 348, L54
Dauser T., García J., Walton D. J., Eikmann W., Kallman T., McClintock J., Wilms J., 2016, A&A, 590, A76
Davis S. W., Done C., Blaes O. M., 2006, ApJ, 647, 525
de La Calle Pérez I. et al., 2010, A&A, 524, A50
Done C., Madejski G. M., Życki P. T, 2000, ApJ, 536, 213
Done C., Gierliński M., Kubota A., 2007, A&AR, 15, 1
Done C., Davis S. W., Jin C., Blaes O., Ward M., 2012, MNRAS, 420, 1848
Elvis M. et al., 1994, ApJS, 95, 1
Esin A. A., McClintock J. E., Narayan R., 1997, ApJ, 489, 865
Fabian A. C., Iwasawa K., Reynolds C. S., Young A. J., 2000, PASP, 112, 1145
Freeman P., Doe S., Siemiginowska A., 2001, in Starck J.-L., Murtagh F. D., eds, Proc. SPIE Conf. Ser., Vol. 4477, Astronomical Data Analysis. SPIE, Bellingham, p. 76
Gaskell C. M., 2017, MNRAS, 467, 226
Gaskell C. M., Benker A. J., 2007, preprint (arXiv:0711.1013)
Holt S. S., Turner T. J., Mushotzky R. F., Weaver K., 1989, ESASP, 296, 1105

Jin C., Ward M., Done C., Gelbord J., 2012, MNRAS, 420, 1825
Koratkar A., Blaes O., 1999, PASP, 111, 1
Kubota A., Done C., 2018, MNRAS, 480, 1247
Lang D., Hogg D. W., Mierle K., Blanton M., Roweis S., 2010, AJ, 139, 1782
Magdziarz P., Blaes O. M., Zdziarski A. A., Johnson W. N., Smith D. A., 1998, MNRAS, 301, 179
Mahmoud R. D., Done C., 2020, MNRAS, 491, 5126
Malkan M. A., 1983, ApJ, 268, 582
Malkan M. A., Jensen L. D., Rodriguez D. R., Spinoglio L., Rush B., 2017, ApJ, 846, 102
Mantovani G., Nandra K., Ponti G., 2016, MNRAS, 458, 4198
Markowitz A., 2009, ApJ, 698, 1740
Marziani P., Calvani M., Sulentic J. W., 1992, ApJ, 393, 658
McClintock J. E., Remillard R. A., 2006, in Lewin W., van der Klis M., eds, Compact stellar X-ray sources, Cambridge Astrophysics Series, No. 39. Cambridge University Press, Cambridge, UK, p. 157
McKernan B., Yaqoob T., 2004, ApJ, 608, 157
Mehdipour M., Costantini E., 2018, A&A, 619, A20
Mehdipour M., Branduardi-Raymont G., Page M. J., 2012, A&A, 542, A30
Mehdipour M. et al., 2015, A&A, 575, A22
Miller J. M., 2007, ARA&A, 45, 441
Nandra K., O'Neill P. M., George I. M., Reeves J. N., 2007, MNRAS, 382, 194
Narayan R., Yi I., 1994, ApJ, 428, L13
Noda H., Done C., 2018, MNRAS, 480, 3898
Novikov I. D., Thorne K. S., 1973, Black Holes (Les Astres Occlus), p. 343
Ogawa S., Ueda Y., Yamada S., Tanimoto A., Kawaguchi T., 2019, ApJ, 875, 115
Osterbrock D. E., Ferland G. J., 2006, agna.book
Page M. J. et al., 2012, MNRAS, 426, 903
Perola G. C. et al., 2002, A&A, 389, 802
Petre R., Mushotzky R. F., Krolik J. H., Holt S. S., 1984, ApJ, 280, 499
Petrucci P. O. et al., 2020, A&A, 634, A85
Piro L., Yamauchi M., Matsuoka M., 1990, ApJL, 360, L35
Porquet D. et al., 2018, A&A, 609, A42
Postma J. E., Leahy D., 2017, PASP, 129, 115002
Schlafly E. F., Finkbeiner D. P., 2011, ApJ, 737, 103
Shang Z. et al., 2005, ApJ, 619, 41
Singh K. P., Rao A. R., Vahia M. N., 1991, ApJ, 377, 417
Singh K. P. et al., 2014, Proc. SPIE Conf. Ser. Vol. 9144, Space Telescopes and Instrumentation 2014: Ultraviolet to Gamma Ray. SPIE, Bellingham, 91441
Tandon S. N. et al., 2017, AJ, 154, 128
Tandon S. N. et al., 2020, AJ, 159, 158
Tripathi P., Dewangan G. C., Papadakis I. E., Singh K. P., 2021, ApJ, in press (arXiv:2104.13031)
Vanden Berk D. E. et al., 2001, AJ, 122, 549
Vasudevan R. V., Fabian A. C., Gandhi P., Winter L. M., Mushotzky R. F., 2010, MNRAS, 402, 1081
Véron-Cetty M. P., Véron P., 2006, A&A, 455, 773
Willmer C. N. A., Focardi P., Chan R., Pellegrini P. S., da Costa N. L., 1991, AJ, 101, 57
Winge C., Peterson B. M., Pastoriza M. G., Storchi-Bergmann T., 1996, ApJ, 469, 648

This paper has been typeset from a TEX/LATEX file prepared by the author.